

# Submicrometre-resolution polychromatic three-dimensional X-ray microscopy

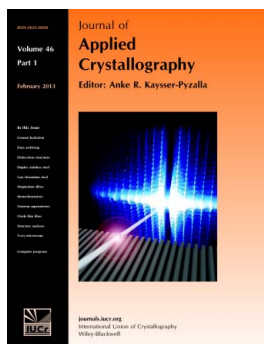
**B. C. Larson and L. E. Levine**

*J. Appl. Cryst.* (2013). **46**, 153–164

Copyright © International Union of Crystallography

Author(s) of this paper may load this reprint on their own web site or institutional repository provided that this cover page is retained. Reproduction of this article or its storage in electronic databases other than as specified above is not permitted without prior permission in writing from the IUCr.

For further information see <http://journals.iucr.org/services/authorrights.html>



*Journal of Applied Crystallography* covers a wide range of crystallographic topics from the viewpoints of both techniques and theory. The journal presents papers on the application of crystallographic techniques and on the related apparatus and computer software. For many years, the *Journal of Applied Crystallography* has been the main vehicle for the publication of small-angle scattering papers and powder diffraction techniques. The journal is the primary place where crystallographic computer program information is published.

Crystallography Journals **Online** is available from [journals.iucr.org](http://journals.iucr.org)

# Submicrometre-resolution polychromatic three-dimensional X-ray microscopy<sup>1</sup>

B. C. Larson<sup>a\*</sup> and L. E. Levine<sup>b</sup>Received 7 June 2012  
Accepted 22 October 2012

<sup>a</sup>Materials Science and Technology Division, Oak Ridge National Laboratory, Oak Ridge, TN 37831-6118, USA, and <sup>b</sup>Material Measurement Laboratory, National Institute of Standards and Technology, Gaithersburg, MD 20899-8553, USA. Correspondence e-mail: larsonbc@ornl.gov

The ability to study the structure, microstructure and evolution of materials with increasing spatial resolution is fundamental to achieving a full understanding of the underlying science of materials. Polychromatic three-dimensional X-ray microscopy (3DXM) is a recently developed nondestructive diffraction technique that enables crystallographic phase identification, determination of local crystal orientations, grain morphologies, grain interface types and orientations, and in favorable cases direct determination of the deviatoric elastic strain tensor with submicrometre spatial resolution in all three dimensions. With the added capability of an energy-scanning incident beam monochromator, the determination of absolute lattice parameters is enabled, allowing specification of the complete elastic strain tensor with three-dimensional spatial resolution. The methods associated with 3DXM are described and key applications of 3DXM are discussed, including studies of deformation in single-crystal and polycrystalline metals and semiconductors, indentation deformation, thermal grain growth in polycrystalline aluminium, the metal–insulator transition in nanoplatelet VO<sub>2</sub>, interface strengths in metal–matrix composites, high-pressure science, Sn whisker growth, and electromigration processes. Finally, the outlook for future developments associated with this technique is described.

© 2013 International Union of Crystallography  
Printed in Singapore – all rights reserved

## 1. Introduction

Polychromatic three-dimensional X-ray microscopy (3DXM) with submicrometre spatial resolution is a powerful technique for probing the structure and microstructure of crystalline materials on mesoscopic length scales – providing a critical bridge linking the nanoscale structure of materials with the macroscale continuum structure. The development of capabilities for using submicrometre-resolution 3DXM over length scales of up to a hundred micrometres has been made possible over the past 15 years by ongoing revolutions in the brilliance of synchrotron X-ray sources, the development of high-precision hard X-ray focusing optics, increases in the speed and resolution of X-ray area detectors, and the advent of fast parallel-architecture computers with multi-terabyte storage systems. By combining 3DXM with the complementary technique high-energy diffraction microscopy, which uses monochromatic X-rays (50–100 keV) and rotating samples to achieve a few micrometre spatial resolution over length scales of up to a millimetre, as reviewed by Poulsen *et al.* (2004) and Poulsen (2004), it is now possible to probe the evolution of the

structure and microstructure of materials nondestructively on length scales ranging from submicrometre to millimetre and beyond. Just as revolutionary developments in transmission electron microscopy (which began over 60 years ago) continue at a rapid pace today, the flow of new developments in spatially resolved hard X-ray microscopy capabilities can be expected to continue into the foreseeable future. Accordingly, it is important to keep in mind that the impact of X-ray microscopies on the fundamental understanding of materials and on advances in materials technology is yet to be fully appreciated.

In this review, we will recall the development of submicrometre-resolution polychromatic 3DXM and briefly describe the differential-aperture (knife-edge) depth-profiling technique that is key to submicrometre spatial resolution in three dimensions. While this is not a comprehensive technical review, the range of accomplishments associated with 3DXM will be discussed, including elastic and plastic deformation in metals and semiconductors, grain growth in polycrystals, local structure and strain in oxide buffer layers, whisker growth in solders, and nanostructure crystallography. We will conclude with a perspective on future developments of the technique and the anticipated impact on understanding the science of materials on mesoscopic length scales.

<sup>1</sup> This article forms part of a special issue dedicated to advanced diffraction imaging methods of materials, which will be published as a virtual special issue of the journal in 2013.

## 2. Polychromatic 3DXM background and methods

Polychromatic 3DXM exploits the development of achromatic elliptically figured Kirkpatrick–Baez (K–B) geometry mirrors that focus hard X-rays to a point, independent of their wavelength. Achromatic focusing optics are a critically important aspect because the crystallographic basis of polychromatic 3DXM is that of Laue diffraction, which requires a wide bandpass ( $\sim 5\text{--}25$  keV) of X-ray energies to generate full polychromatic diffraction patterns at each point along the microbeam. Progress in achromatic focusing optics for hard X-rays has been discussed in a recent review (Ice *et al.*, 2011) and in a recent paper (Liu *et al.*, 2012); key Laue diffraction aspects associated with 3DXM were discussed by Chung & Ice (1999) in relation to the analysis of white-beam microdiffraction patterns to extract local crystal structure, orientation and deviatoric (*i.e.* non-volumetric, shape distortion) strain. They further discussed the use of an (insertable/removable) energy-scanning monochromator to perform scanned monochromatic microbeam measurements for the determination of lattice parameters and dilatational (volumetric) strain. Combining white-beam deviatoric strain measurements with scanned monochromatic dilatational strain measurements on a single Bragg reflection provides access to full strain tensors.

### 2.1. Two-dimensional X-ray microscopy

Although this review is directed toward polychromatic 3DXM, it is instructive to include polychromatic two-dimensional X-ray microscopy (2DXM) as well because the crystallographic analyses of 2DXM and depth-resolved 3DXM

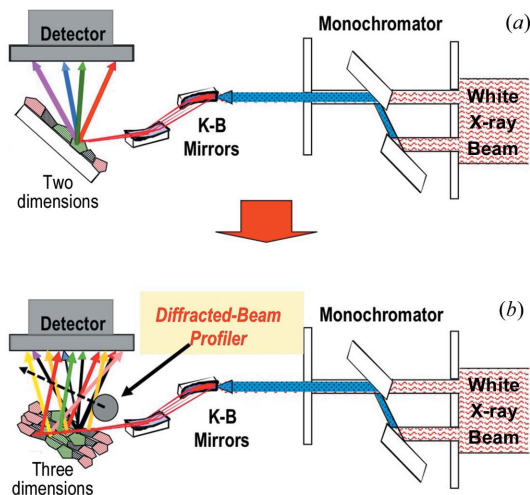


**Figure 1** Schematic view of two-dimensional and three-dimensional X-ray microscopy. (a) White synchrotron X-rays are either passed to K–B mirrors with the monochromator removed or double-Bragg reflected as monochromatic X-rays to the K–B mirror. The focused microbeam strikes the sample and produces either a polychromatic Laue pattern on the detector or a single monochromatic Bragg reflection. (b) Same as (a), but with a Pt diffracted-beam profiler wire to provide spatial resolution in three dimensions. Adapted from Yang, Larson, Tischler *et al.* (2004) with permission.

diffraction patterns are the same (see Fig. 1); the experimental X-ray beamline infrastructure (*e.g.* white beam, K–B mirror focusing) is common to both techniques; and there are strong overlaps in the science. For thin films, the local crystal structure, crystallographic orientations and deviatoric strain tensors can be obtained directly through the analysis of white-beam Laue diffraction patterns, where the spatial resolution is determined by the diameter of the K–B mirror-focused microbeam. As illustrated schematically in Fig. 1(a), the basis for 2DXM is that of submicrometre-focused polychromatic beams, precision two-dimensional stages to scan samples and high-resolution X-ray area detectors. This infrastructure is combined with automated X-ray Laue pattern recognition software with the ability to determine the crystal structure, the local crystallographic orientation and deviatoric strains through determinations of how the angles between Laue spots deviate from those for perfect crystal symmetry. Driven by the importance of thin-film materials in fundamental science and technology-related applications, the direct sensitivity of X-rays to elastic and plastic strains (Spolenak *et al.*, 2010), and the relatively straightforward implementation of the technique with polychromatic microbeams, 2DXM is available at many synchrotron sources around the world with computer-automated diffraction pattern recognition and crystallographic analysis software such as the microbeam software developed at the Advanced Photon Source (APS) and the XMAS package developed at the Advanced Light Source (ALS) (see tutorial by Polvino *et al.*, 2012).

### 2.2. Three-dimensional X-ray microscopy

Nondestructive submicrometre-resolution spatially resolved measurements of crystal structures, orientations, local microstructure and strain tensors in the interior of bulk materials have been a long-standing goal in order to interrogate the structure, microstructure and evolution of materials on mesoscopic length scales. The extension from 2DXM to 3DXM is not straightforward as it entails the extraction of submicrometre-resolution depth-resolved Laue diffraction patterns from all positions along a microbeam (Larson *et al.*, 2002). The ability to disentangle the inherently ‘depth-integrated’ superposition of Laue patterns on detectors is key to 3DXM as a nondestructive probe of the structure and microstructure of materials. Larson *et al.* (2002) developed a knife-edge (or differential-aperture) depth-profiling technique that makes it possible to reconstruct depth-resolved Laue diffraction patterns by collecting diffraction images on an area detector while stepping a cylindrical platinum wire ( $\sim 50$   $\mu\text{m}$  diameter) with submicrometre step sizes through the diffraction pattern. Unfortunately, a straightforward submicrometre slit cannot be used for this purpose. This is because slits used with hard ( $> 10$  keV) X-rays must be at least  $\sim 10$   $\mu\text{m}$  thick to be X-ray opaque, and as illustrated in Fig. 2, submicrometre-width slits with a thickness of 10  $\mu\text{m}$  correspond to a collimator that passes only a narrow range of angles (less than 6) rather than the required  $> 45$  range of angles associated with Laue diffraction patterns. Moreover, the circular cross section

of the profiling wire for this so-called ‘differential-aperture’ depth-profiling technique is important; this ensures that the absorption geometry of the profiler is independent of the angle of the diffracted X-rays.

By collecting Laue images on the area detector after each step of the profiling wire and performing a pixel-by-pixel digital subtraction of detector images from successive steps to obtain difference images, it is possible to determine the source point along the X-ray microbeam of each Bragg peak, as illustrated in Fig. 2. Geometric triangulation from the position of pixels containing Bragg peaks on the detector to the tangent point on the profiling wire determines the direction of the X-rays; extrapolating to the depth of the microbeam then determines the source position of the X-ray scattering in the difference images. Fig. 3 shows schematically that the parallax in the source point associated with the width of the detector pixels is not significant down to profiler wire step sizes of  $\sim 0.5 \mu\text{m}$  for typical detector and scattering geometry conditions (for details, see Yang, Larson, Tischler *et al.*, 2004). The change in intensity for pixels containing Bragg peaks as the wire is step-advanced corresponds to the amount of intensity

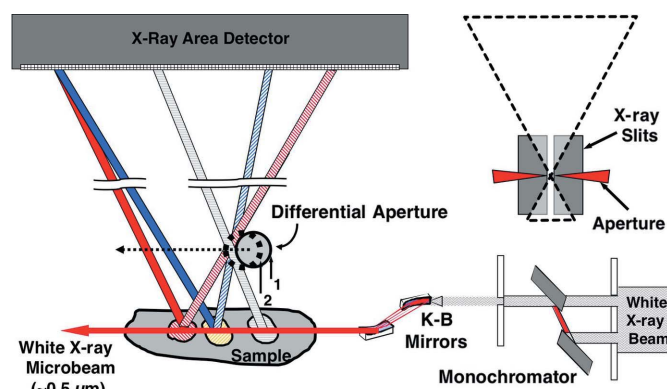


**Figure 2**

Schematic drawing of a  $50 \mu\text{m}$  differential-aperture depth-profiler wire occluding Bragg-reflected X-rays from a wide range of angles. The angular range of the reflections from various positions along the beam would not pass through a narrow slit, which acts like a collimator rather than an aperture.

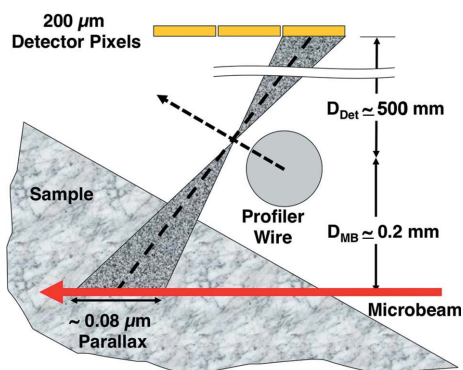


**Figure 3**

Schematic view of the small size of the measurement parallax along the beam as a result of the much greater distance from the profiler to the detector pixels than from the profiler to the microbeam. Adapted from Yang, Larson, Tischler *et al.* (2004) with permission.

scattered from individual source points. As explained in detail elsewhere (Larson *et al.*, 2008, 2002; Yang *et al.*, 2003; Yang, Larson, Pharr *et al.*, 2004; Yang, Larson, Tischler *et al.*, 2004), by collating these difference images as a function of depth for each step of the profiling wire it is possible to computationally ‘reconstruct’ the pixel intensities into depth-resolved Laue diffraction patterns (*i.e.* detector images) for all depth positions along the beam, as implied schematically in Fig. 4 for polycrystalline aluminium.

By design, these depth-resolved reconstructed images are in a form that can be analyzed directly in terms of the crystal structure, orientation and deviatoric strain using the same crystallographic software as for the 2DXM case. As with the two-dimensional case, obtaining dilatational as well as deviatoric strains requires a depth-resolved monochromatic energy scan for at least one Bragg reflection at each depth in addition to the polychromatic depth-resolved Laue patterns. As discussed in the next subsection, such measurements are referred to as scanned monochromatic three-dimensional X-ray microscopy (SM-3DXM), a technique that is complementary to polychromatic 3DXM as well as a source of additional information to obtain lattice parameters and dilatational strains.

### 2.3. Scanned monochromatic three-dimensional X-ray microscopy

The polychromatic Laue diffraction measurement technique discussed above provides crystal symmetry, orientation and unit-cell shape information but does not provide the lattice parameters or unit-cell volumes. That is the reason for the monochromator in Fig. 1, which can be either inserted into the white beam to direct monochromatic X-rays onto the

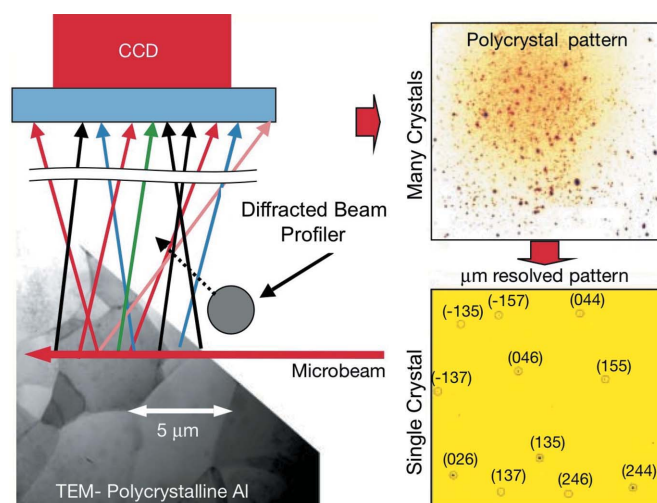


**Figure 4**

Schematic illustration depicting the result of reconstructing the polychromatic Laue diffraction patterns as a function of depth along the beam by differential-aperture depth profiling and subsequent collation of difference images calculated between successive steps of the profiler wire. The depth-integrated random-like spot pattern becomes a series of single-crystal Laue patterns corresponding to the grain at that depth. Adapted from Larson *et al.* (2002) with permission.

focusing mirrors or removed to allow white X-rays to be focused onto the sample. When the monochromator is inserted, X-rays from the lower part of the synchrotron beam are Bragg reflected from the bottom crystal up to the second crystal of the narrow-gap double monochromator and then Bragg reflected along the same path that the white beam travels when the monochromator is not inserted. After indexing white-beam Laue diffraction patterns, the nominal energy for Bragg reflection for each of the typically 10–30 Laue reflections measurable on the area detector can be calculated using beamline crystallographic software.

As demonstrated by Yang *et al.* (2003) in Fig. 5 for the case of a cylindrically-bent thin silicon plate, it is possible to perform a nested X-ray energy (monochromator) and depth (profiler wire) scan on any of the reflections to determine the Bragg angle and Bragg energy as a function of depth along the microbeam. Because of the angular convergence of the focused microbeam, energy steps of around 1–3 eV are typical, with  $\sim 10$ –20 energy steps for each step of the wire depth profiler. When used in connection with white-beam 3DXM measurements, the lattice parameter of only one reflection is required per depth increment (Chung & Ice, 1999).

### 3. Applications of submicrometre-resolution 3DXM

The initial application of differential-aperture 3DXM by Larson *et al.* (2002) using polychromatic focused X-ray microbeams demonstrated that full diffraction patterns could be obtained with micrometre depth resolution in three dimensions for the cases of 5  $\mu\text{m}$ -grain-size polycrystalline aluminium and an elastically bent thin silicon plate. This process is illustrated schematically in Fig. 4, where local crystal orientations as a function of depth along the microbeam are extracted in the form of discrete single-crystal Laue patterns in the depth-profiling analysis of the highly superposed poly-

crystalline Laue diffraction patterns. Analogous depth-resolved measurements on cylindrically bent Si in the initial paper by Larson *et al.* (2002) and later by Larson *et al.* (2008) demonstrated further that not only local crystal orientations but also deviatoric strain could be extracted with micrometre depth resolution when the orientations change continuously as a function of distance along the microbeam. The demonstration that quantitative measurements of the deviatoric strain tensor and the total strain tensor (*i.e.* deviatoric plus dilatational strain) could be extracted with micrometre depth resolution and  $10^{-4}$  strain resolution under continuously varying strain implies the ability to extract both intra- and intergranular strain tensors and local crystal orientations with micrometre three-dimensional resolution near grain boundaries in elastically strained polycrystalline materials.

As discussed in more detail below, however, caution must be used for cases in which inhomogeneous plastic deformation (*i.e.* containing dislocation patterning and slip traces) is involved as well as elastic deformation. The asterism and/or streaking of Laue spots resulting from irregular (*i.e.* not smoothly varying) rotations on length scales below the measurement resolution volume tend to increase uncertainties in deviatoric strain tensor measurements significantly in comparison with elastic strain in dislocation-free brittle materials.

#### 3.1. 3DXM investigations of deformation and microstructure evolution in crystalline materials

The nondestructive capabilities of 3DXM for probing local crystal structure, local orientations, and local elastic and plastic strains on mesoscopic length scales (submicrometre to tens and hundreds of micrometres) are extremely important for the investigation of fundamental aspects of deformation and grain growth in crystalline materials. Although deformation processes are a major cause of failure in structural materials, highly refined deformation processing of metals represents one of the oldest and most important materials processing procedures (Hu *et al.*, 1992; Kelkar *et al.*, 2001). Both ductile failure and deformation processing are dominated by complex and collective dislocation interactions on mesoscopic length scales (Kubin, 1993). Therefore, the capability for directly and nondestructively measuring local crystallographic rotations and elastic strains makes 3DXM a unique and powerful tool for fundamental investigations of deformation through measurements of local elastic strain and so-called geometrically necessary dislocation (GND) densities in deformed materials. GNDs are associated with the local rotational and dilatational fluctuations generated by local variations in the net Burgers vector content and local strains associated with dislocation distribution fluctuations within deformed materials. As such, 3DXM provides previously unavailable nondestructive measurements of dislocation generation, aggregation and evolution on mesoscopic length scales. Such measurements provide a window into the complex and collective effects associated with plastic deformation and the extent to which deformation impacts on local crystal-

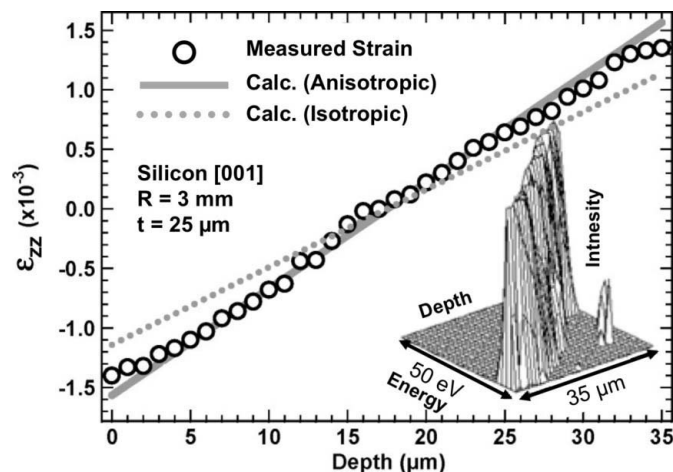


**Figure 5** Comparison of scanned monochromatic 3DXM measurements and calculations of surface normal strain in a 25  $\mu\text{m}$ -thick silicon plate bent elastically to a radius of 3 mm. The inset shows the sharply peaked Bragg intensity as a function of monochromator energy and depth along the microbeam in the bent plate. Adapted from Yang *et al.* (2003) with permission.

lographic and mechanical properties (Mughrabi & Ungár, 2002; Zaiser & Seeger, 2002).

**3.1.1. Elastic and plastic deformation in bent Si plates.** The dislocation density tensor,  $\alpha_{ij}$ , introduced originally by Nye (1953) for rotations [and generalized later to include elastic strains; see Kröner (1981)], provides a quantitative spatially localized measure of the GND density required to accommodate lattice curvature and elastic strain in deformed materials (Needleman & Sevillano, 2003, and references therein). Defined mathematically (El-Azab, 2000) in terms of the difference between the local lattice curvature (*i.e.* three-dimensional rotation gradients) and the curl of the local elastic strain (*i.e.* three-dimensional strain gradients), GND densities are given numerically by the norm of the dislocation tensor divided by the Burgers vector (Larson *et al.*, 2008, 2007). For dislocation-free elastic bending of brittle materials, the lattice curvature is accommodated entirely by elastic strains, while in elastically soft materials bending deformation is accommodated largely by the introduction of dislocations due to low yield strengths. With the ability to measure both local lattice rotations and elastic strains nondestructively, 3DXM is ideally suited for GND determinations. The first demonstration of nondestructive three-dimensional measurements of GND densities in terms of the dislocation tensor with micrometre

resolution was performed on deformed thin (42 and 25  $\mu\text{m}$  thickness) silicon plates using 3DXM (Larson *et al.*, 2008). Using the geometries shown in Fig. 6, micrometre-spatial-resolution 3DXM measurements of local orientations and strains were made in the  $yz$  planes of an elastically bent Si plate and a similar, but plastically deformed, Si plate (Larson *et al.*, 2008). GND densities were determined in the Si plate bent elastically to a radius of 5 mm (Fig. 6a) and in the similarly bent plate (Fig. 6b) after annealing to 973 K (*i.e.* plastically deformed by heating above the brittle-to-ductile transformation temperature under the bending stress). The spatially resolved dislocation tensor components,  $\alpha_{ij}$ , plotted in Fig. 6 were determined directly from the gradients of the rotations and strains measured by 3DXM, which were in turn extracted by numerical differentiation of the spatially resolved orientation and strain measurements (Larson *et al.*, 2008).

As expected for a brittle material, no significant densities of GNDs were found in the elastically bent Si sample after removing measurement noise. However, the sample that was bent plastically  $\sim 373$  K above the brittle-to-ductile transformation temperature contained strong inhomogeneously distributed bands of GNDs lying along  $\{111\}$  slip-plane traces in the  $\alpha_{xy}$  component and somewhat lower GND densities in the  $\alpha_{xz}$  component, along with activity to a lesser degree in

other components. The presence of low-density GNDs in several components suggests the presence of more complex local slip activity and, to some extent, the inherent presence of uncertainties in extracting numerical derivatives from local orientation measurements.

This nondestructive and quantitative GND density measurement capability of 3DXM has strong implications for fundamental investigations of deformation on mesoscopic length scales. It is possible to perform direct quantitative tests of crystal plasticity and discrete dislocation dynamics simulations of deformation. We note that GND densities are a function of local lattice curvature and, hence, are inherently a function of the spatial step size of the probing measurements. Accordingly, direct and absolute comparisons of measurements of GND densities with GND simulations require coarse graining of calculations with a resolution that matches that of the curvature and strain experimental measurements.

**3.1.2. Deformation correlations in tensile-deformed Cu single crystals.** The inhomogeneous and multiple-length-scale fluctuating nature of deformation in ductile materials

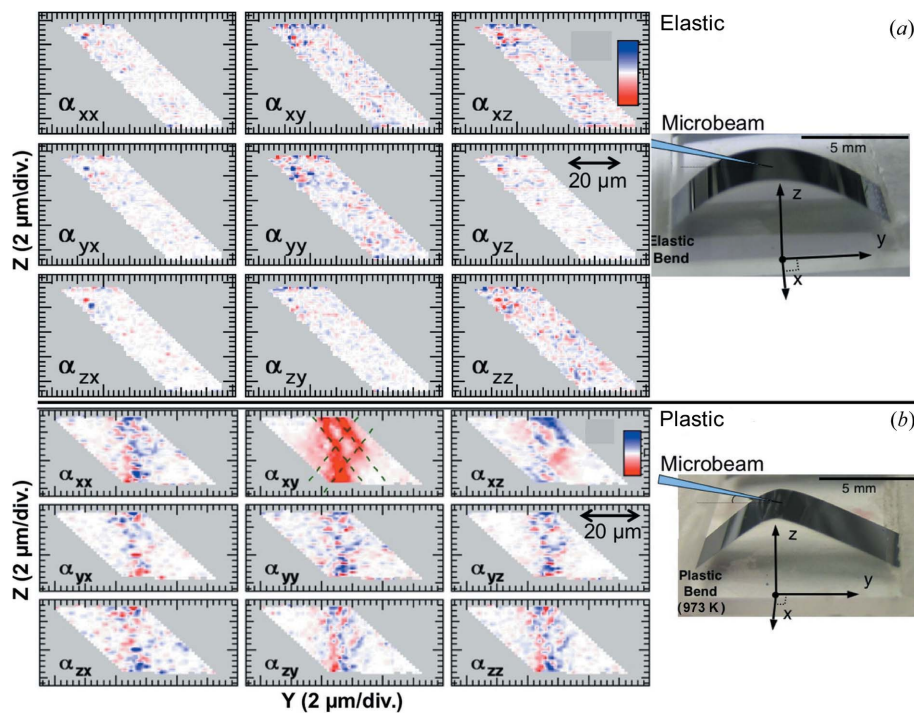


**Figure 6**

Photographs of a 42  $\mu\text{m}$ -thick silicon plate bent elastically to a 5 mm radius (*a*) and a 25  $\mu\text{m}$ -thick silicon plate bent plastically by heating to 973 K under bending stress (*b*). The left side of the figure shows micrometre-resolution spatially resolved measurements of dislocation tensor components for (*a*) the elastically bent silicon plate and (*b*) the plastically bent silicon plate. Within statistical uncertainties, the elastically bent case (*a*) has no GNDs. The plastically bent case (*b*) indicates strong bands (red) of GNDs in the  $\alpha_{xy}$  component and smaller density distributions (blue and red) in the  $\alpha_{xz}$  component. Weaker but nonzero densities are visible in the remaining components as well. The dashed lines in the  $\alpha_{xy}$  component of (*b*) correspond to two of the  $\{111\}$  plane traces, indicating that the plastic deformation is concentrated largely on these slip directions. The full-scale magnitudes of the GNDs in the color scale correspond to  $\rho = 0.95 \times 10^9 \text{ cm}^{-2}$ . Adapted from Larson *et al.* (2008) with permission.

suggests that statistical as well as local analyses of three-dimensional deformation measurements will be required in order to make quantitative comparisons of experiments with theory and simulations. Pang *et al.* (2010) performed the first three-dimensional spatial correlation analysis on deformation-induced misorientations using micrometre-resolution 3DXM deformation measurements on single-crystal Cu crystals deformed 8% in tension along the [123], [111] and [001] directions. The angular misorientations showed self-affine behavior for length scales (correlation lengths) of  $\sim 70\ \mu\text{m}$  for the single-slip [123] orientation compared with only  $\sim 15\text{--}20\ \mu\text{m}$  for the multi-slip [111] and [001] orientations. The significantly longer correlation length for the easy-glide single-slip direction indicates the disruptive impact of multiple-slip-plane deformation for face-centered-cubic materials. The spatial correlation analysis of the misorientations further provided a measure of the so-called Hurst exponent ( $0 < H < 1$ ) (Zaiser & Moretti, 2005), characterizing whether the spatial correlations within the sample are positive ( $H > 0.5$ ), negative ( $H < 0.5$ ) or random ( $H = 0.5$ , uncorrelated). Interestingly, values of  $H = 0.72$  were found at the sample surface for each strain direction; this is similar to the results simulated by Zaiser & Moretti (2005) for surface roughness in deformed crystalline materials. On the other hand,  $10\ \mu\text{m}$  below the surface of deformed Cu,  $H$  was found to decrease smoothly to  $H \simeq 0.7, 0.47$  and  $0.32$  for the [123], [111] and [001] directions, respectively. The positive rotation correlations for single-slip deformation and anticorrelations for the strong multi-slip [001] direction are understandable qualitatively in terms of the intersection of slip on active slip planes in the bulk and the (geometrically limited) absence of slip intersections at the surface. The quantitative nature of the measurements and the near-surface spatial dependence of the correlations provide an opportunity for quantitative theoretical predictions and simulation of deformation and dislocation patterning on mesoscopic length scales.

### 3.1.3. Dislocation structures in heavily deformed metals.

The formation and evolution of dislocation structures (patterning, dislocation cell structures) at the subgrain length scale is one of the most important aspects of the deformation process in ductile metals. Although it is generally appreciated that patterning arises from the collective interactions of dislocations (Hahner & Zaiser, 1999; Argon & Haasen, 1993; Thomson & Levine, 1998; Levine *et al.*, 2006), it is not yet possible to predict the evolution of dislocation distributions and the resulting local stresses. Such understanding is a crucial foundation for developing trustworthy models for material deformation.

Stresses in materials cannot be measured directly. However, since SM-3DXM can measure absolute lattice parameters, comparison with the unstrained lattice spacing provides a direct measure of the elastic strain, which can in turn be converted to a stress using the stiffness tensor for the material. The first proof-of-principle demonstration that SM-3DXM can be used to measure local elastic strains was performed by Yang *et al.* (2003) on a cylindrically (elastic) bent thin plate of silicon. The first use of this technique to measure elastic strains

within the dislocation microstructure of plastically deformed metal specimens was by Levine *et al.* (2006) on two unloaded single-crystal Cu samples that had been deformed in tension and compression (each) by 25% along the (001) axes. Using the axial 006 reflection, the average axial elastic strain was measured for a number of different dislocation cell interiors from both samples. The cell interiors of the tensile-deformed specimen were found to be in compression and those in the compression-deformed specimen were in tension. This counterintuitive result confirmed the long-standing composite model of plastic deformation that had been proposed by Mughrabi (1983) more than 20 years earlier. Equally importantly, these first spatially resolved measurements showed an unpredicted dramatic variation of strains from cell to cell within the sample.

More recently, Levine *et al.* (2011) combined submicrometre-spatial-resolution SM-3DXM with diffracted-beam masking of selected detector pixels to make (several hundred) direct measurements of axial elastic strain in individual dislocation cell walls and their adjacent cell interiors in heavily deformed (28% strain in compression) single-crystal copper. Converting to axial [001] stresses using the elastic modulus in the [001] direction,  $E_{001}$ , these data are combined in Fig. 7 to show the volume-normalized stress distribution functions for dislocation cell walls and cell interiors. These spatially resolved measurements showed broad asymmetric distributions of dipolar stresses that are markedly displaced from one another. Comparison with detailed deformation models demonstrated that the distribution of local stresses is consistent with random trapping of mobile dislocations by dislocation walls.

These SM-3DXM measurements of elastic strains in deformed metals have already answered numerous long-standing fundamental questions about metals deformation, as discussed in a recent comprehensive contextual review by Kassner *et al.* (2012). Extending these results to larger length scales requires consideration of the interaction of dislocations

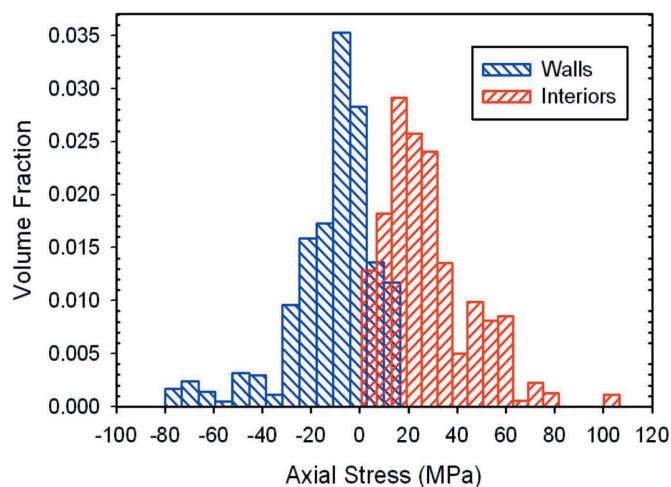


**Figure 7** Axial stresses within individual dislocation cell walls and cell interiors in copper single crystals deformed in compression by 28%. Adapted from Levine *et al.* (2011) with permission.

with interfaces such as grain boundaries in polycrystalline materials. Such studies could then address real-world engineering problems. An example of how polychromatic 3DXM has provided new insights on damage nucleation at this larger length scale was published recently by Wang *et al.* (2011). In that work, the role of twinning on damage nucleation was studied in commercial purity titanium strained to 1.5%. Using 3DXM measurements, the dislocation activity associated with forming T2 twins was investigated by quantitative analysis of the streaked shapes of various Bragg peaks within the spatially resolved Laue diffraction patterns.

Another important capability of 3DXM is that of assessing volume-averaged diffraction measurements. It should be remembered that the vast majority of X-ray diffraction measurements performed around the world have spatial resolutions larger than the microstructural features that are being explored. Thus, critical assumptions are often implicit in interpretations of these measurements. In a recent study, Levine *et al.* (2012) used SM-3DXM to directly test long-standing assumptions that are used to analyze volume-averaged X-ray line profiles from deformed metals (Ungár *et al.*, 1984; Mughrabi *et al.*, 1986). Submicrometre-resolution diffraction data obtained from the dislocation microstructures responsible for the volume-averaged profiles showed that, without additional constraints, the traditional volume-averaged analyses can produce ambiguous results.

#### 3.1.4. Thermal grain growth in polycrystalline aluminium.

One of the long-standing issues in technological processing of structural materials is that of understanding and predicting the three-dimensional process of recrystallization and grain growth on mesoscopic length scales following rolling or other deformation steps. Accordingly, the possibility of nondestructively monitoring the thermodynamics-driven evolution of polycrystalline grains with submicrometre spatial resolution was one of the driving forces for the development of polychromatic 3DXM. Fig. 8 shows 3DXM measurements of grain

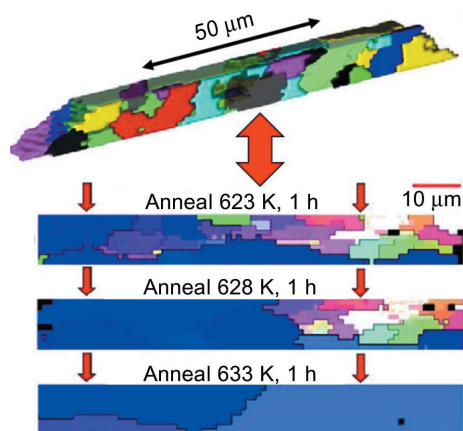


**Figure 8**

False color plots of crystal grains in polycrystalline Al. The three-dimensional picture shows the volume of polycrystalline Al investigated with polychromatic 3DXM. The three slices below are false color plots of the grain sizes on a particular slice of the three-dimensional volume after isochronal annealing at 623, 628 and 633 K for 1 h between measurements. Adapted from Budai *et al.* (2008) with permission.

evolution in a  $10 \times 10 \times \sim 100 \mu\text{m}$  volume of Al after 1 h annealing steps between 623 and 633 K (Budai *et al.*, 2008). Clearly, the grain-coarsening process for this 473 K hot-rolled 1000 series polycrystalline Al with  $\sim 5 \mu\text{m}$  grain size involves processes with broad crystal growth fronts overtaking smaller grains in addition to local grain boundary orientation and local grain boundary curvature effects. Analysis procedures for three-dimensional point-to-point micrometre- or submicrometre-resolution data in terms of grain boundary orientations, boundary types and coincidence-site orientations have been developed, as have software routines to assess local drivers such as dislocation density and intragranular defects that can impact grain boundary motion. Unfortunately, as shown in the 633 K anneal panel, the impingement of fast growing grains from outside the original volume scanned by 3DXM limits the ability to model or understand such processes because of lack of knowledge about the initial source of these fast growing grains. Procedures to increase the speed of such three-dimensional measurements through faster detectors and optimized analysis routines have now been implemented at the APS, and significantly larger volumes are being analyzed. This will provide databases appropriate for direct predictive computational analyses (see Rollett *et al.*, 2007; Olmsted *et al.*, 2009).

**3.1.5. Deformation under micro-indentations.** One of the important aspects of 3DXM is the ability to make local misorientation and strain measurements with high spatial resolution. However, the heterogeneous nature of deformation in large bulk samples provides a dilemma, with the need to choose between detailed measurements in a small selected volume or less comprehensive measurements averaging over larger volumes. Micro-indentations provide an inherent confinement of deformation within mesoscopic volumes and so provide an alternative option, albeit with spatially varying deformation conditions. Polychromatic 3DXM measurements with micrometre resolution under conical and Berkovich (pyramidal) indents (Yang, Larson, Pharr *et al.*, 2004) demonstrated the confined nature of the deformation field below indents and the ability to perform measurements of the local rotations with high angular precision, and also that the deformation fields below both conical and pyramidal indents possess a hierarchy of local rotations and counter-rotations. Depending on the trajectory of the microbeam through the middle or the periphery of the indents or whether the microbeam trajectory passed directly under the indentation, the microbeam Laue diffraction patterns displayed complex rotational patterns with strong evidence for inhomogeneous dislocation patterning and cell structure characteristic of deformed copper, as discussed above for uniaxially deformed copper (Levine *et al.*, 2006, 2011).

**3.1.6. Mechanical properties of metal–matrix Mo–NiAl composites.** The spatially resolved nature of 3DXM provides a natural capability for investigating mechanical properties in complex materials such as composites. To investigate the mechanical properties of  $\sim 1 \mu\text{m}$ -diameter reinforcing Mo fibers in an Mo–NiAl metal–matrix composite, Barabash *et al.* (2011) used SM-3DXM at the APS to probe (see Fig. 9) the

axial strain distributions in surface-normal-embedded Mo fibers and in Mo fibers exposed by  $\sim 5\ \mu\text{m}$  by selectively etching the matrix. Depth-resolved lattice parameter measurements were made using the 006 reflection along the [001] axial direction of the Mo fiber, as illustrated in the schematic at the top of Fig. 9. Etching the matrix to expose Mo fibers provided an opportunity to measure both the unstressed Mo [001] axial lattice parameter (in the exposed part of the fibers) and the width of the transition region as the fibers enter the matrix. This provided a test of the strength of the interface to maintain the  $-1\%$  differential thermal expansion strain that was generated as the composite cooled from the melt. Using similar measurements on polished but not etched Mo–NiAl surfaces provided a second test of the interface integrity transition depth. The results of measurements for both cases are plotted in Fig. 9. Making use of the geometry, including the  $45^\circ$  angle of the beam with the sample surface and the fibers, the inter-fiber separations in the composite, the coincidence (along the microbeam) of gaps in matrix Bragg reflections with the appearance of fiber Bragg reflections and the position of the onset of matrix Bragg reflections at the surface, Barabash *et al.* (2011) extracted an effective interface strength of  $\sim 180\ \text{MPa}$  and a near-surface slip-zone distance of  $5\ \mu\text{m}$  by fitting to a mechanical model. This slip-zone distance corresponds approximately to the distance over which the fiber strain falls from  $-1\%$  to zero in Fig. 9.

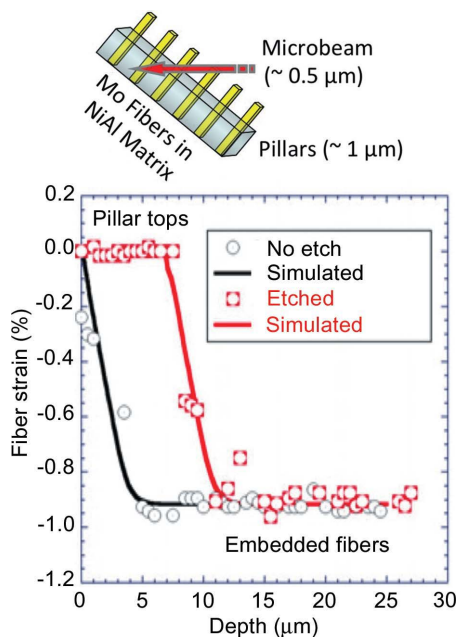


**Figure 9**

The upper schematic drawing illustrates the geometry for scanned monochromatic 3DXM measurements of strain normal to the NiAl matrix face and along the axis of the Mo fibers in an Mo–NiAl metal–matrix composite. The plot below shows the strain in the exposed fibers (square symbols, red line) as a function of depth from the top of the exposed fibers (zero) to  $25\ \mu\text{m}$  deep into the matrix. The gray circles and black line correspond to similar measurements made on a similar sample without etching to expose fibers above the matrix surface. The lines correspond to micromechanical modeling to extract the fiber–matrix interface strength from the depth-dependent fiber strain measurements. Adapted from Barabash *et al.* (2011) with permission.

### 3.2. Depth-integrated 3DXM investigations

3DXM provides the most complete information on the underlying microstructure and evolution of materials under thermodynamic and mechanical driving conditions when used in spatially resolved form. However, when *in situ* conditions or other measurement constraints prevent full three-dimensional studies, it is also possible to obtain a wealth of microstructural information from polychromatic microbeam measurements in bulk materials that cannot be obtained using conventional X-ray diffraction techniques.

**3.2.1. *In situ* deformation in metal pillars.** It has been widely reported that single-crystal face-centered-cubic metal pillars formed using focused ion-beam milling are stronger for smaller sizes (Uchic *et al.*, 2004; Greer & Nix, 2006; Bei *et al.*, 2008; Budiman *et al.*, 2008). Budiman *et al.* (2008) suggested from depth-integrated microbeam Laue measurements that dislocation starvation and not strain hardening led to the apparent added strength of smaller structures. However, Maaß *et al.* (2009), using *in situ* Laue microbeam diffraction (without depth resolution) in combination with crystal plasticity simulations, concluded that plastic deformation is controlled initially by unspecified boundary constraints (*e.g.* preexisting defects, surface damage, misalignment), often leading to initial non-Schmid slip activation during microcompression pillar deformation. Using polychromatic and scanned monochromatic microbeams to study  $2\text{--}10\ \mu\text{m}$ -diameter Au pillars *in situ* under microcompression, it was found that deformation started with a sharp onset of diffraction peak rotation (a so-called ‘Laue yield’) that was followed by classical crystal plasticity corresponding to activation of the highest Schmid factors. Deformation then proceeded with size-dependent strain hardening in what Maaß *et al.* (2009) refer to as percolative slip.

**3.2.2. Indentation size effects.** Although GNDs are in general related to local dislocation density tensors as discussed above (Nye, 1953; Larson *et al.*, 2008, 2007), depth-integrated 3DXM measurements of lattice rotations under the flat faces of pyramidal Berkovich indentations have been used to provide insight into deformation as well (Feng *et al.*, 2008; Barabash *et al.*, 2001). For instance, Feng *et al.* (2008) verified experimentally that the effective strain under self-similar indenters is independent of the indentation depth. This result was further used in connection with the revised Nix–Gao model (Durst *et al.*, 2005) to estimate the size of plastic zones under indents and estimate strain gradients and GNDs without direct depth resolution. The complexity of indent deformation (Yang, Larson, Pharr *et al.*, 2004) suggests that direct depth-resolved measurements will provide more detailed deformation insight.

**3.2.3. Deformation microstructure in bulk deformed copper.** Magid *et al.* (2009) performed depth-integrated polychromatic X-ray microbeam diffraction investigations of large copper single crystals oriented for single slip and compressed uniaxially by approximately 10%. Local deformation patterns were mapped with  $1\text{--}3\ \mu\text{m}$ -diameter white X-ray beams, over large (up to  $297\ \mu\text{m}$  square) regions of samples cut from the interior of the original deformed ingot.

As has been known from etch pit analysis, the deformation is not uniform but strongly concentrated in irregularly spaced bands parallel to {111} planes: in the case studied,  $\sim 30\ \mu\text{m}$  spacing. The depth-integrated polychromatic Laue diffraction patterns provided information on the magnitude of the local lattice rotations integrated over  $\sim 10\text{--}20\ \mu\text{m}$  along the direction of the probing microbeam (limited by photoelectric absorption) as a function of position relative to slip bands in the sample. Magid *et al.* further reported that the analysis of deviatoric strain from the depth-integrated Laue diffraction patterns yielded residual deviatoric stresses significantly exceeding 500 MPa and that the high-stress regions were strongly correlated with the presence of the shear bands. The magnitude of the local stress (strain) state in the material is of course not provided by etch pit analysis; this highlights the importance of microbeam diffraction analyses. However, the presence of strains corresponding to 500 MPa in 10%-compressed Cu is surprising considering that such strains are an order of magnitude larger than those found for 30%-compressed copper using SM-3DXM (Levine *et al.*, 2006, 2011).

As mentioned in connection with the analysis of white-beam diffraction patterns for deformed silicon above and discussed in more detail in the following subsection, experience has shown that considerable caution must be exercised in quantitatively extracting deviatoric strains when even small amounts of asterism or streaking are present in Laue diffraction spots. Considering the fact that the 500 MPa stresses extracted in the 10%-deformed Cu here correlate directly with the presence of shear bands (*i.e.* larger streaks), it is likely that the deviatoric stress magnitudes reported are significantly inflated by diffraction spot distortions. In cases of diffraction spot streaking or distortion, it is suggested that scanned monochromatic (SM-3DXM) measurements of local dilatational strains be used to corroborate the presence of such highly stressed material.

**3.2.4. Uncertainties in the determination of deviatoric strains in deformed materials.** Uncertainties associated with polychromatic deviatoric strain measurements are important as a general issue and so warrant further elaboration. The source of the uncertainty is known to be the slight differences in the streaking and asterism for projections of the local lattice rotations onto different crystal planes. As shown by Larson *et al.* (2002, 2008), 3DXM measurements of both deviatoric and dilatational strain can be performed accurately and precisely in deformed dislocation-free brittle materials such as cylindrically bent Si; however, as pointed out by Larson *et al.* (2008) the same is not true for Si deformed above the brittle-ductile transformation temperature. This is because streaking and asterism cause the centroids of Laue spots to vary as a function of diffraction plane orientation, thus producing spurious deviations in Laue spot position determinations. These streaking/asterism-induced deviations, in turn, introduce spurious angular deviations into the inherently small angular displacements associated with deviatoric strains in ductile materials and hence can exaggerate deviatoric strain values severely.

The Monte Carlo uncertainty analysis of Poshadel *et al.* (2012) addresses such issues in a general way, demonstrating quantitatively the importance of the above-stated uncertainty considerations associated with white-beam deviatoric strain measurements in a tensile-stressed 304 stainless steel wire. Analogously to the caution expressed with respect to stress determinations in deformed Cu (Magid *et al.*, 2009) above and in cyclically deformed nitinol (Robertson *et al.*, 2007) below, Poshadel *et al.* suggest the likelihood of significant artefact-induced uncertainties in the deviatoric strain results reported for plastically deformed quartz (Chen *et al.*, 2011) and a nickel alloy (Chao *et al.*, 2009). Technically the centroids of distorted peaks (especially when used without depth resolution) correspond to an undefined orientation average that is not mathematically related to a direct deviatoric strain measurement.

On the other hand, scanned monochromatic measurements (SM-3DXM) determine strains for single Bragg reflections at a time and are therefore inherently much less sensitive to such effects. Accordingly, 3DXM can provide accurate dilatational strain measurements in the presence of strong diffraction spot distortions, albeit at the cost of performing energy scan measurements for each spot as discussed with respect to results in Fig. 7. Fortunately, polychromatic orientation measurements are also much less impacted by streaking because of the collective nature of Laue spot movements for rotations, in contrast to the differential nature of Laue spot angle changes associated with the extraction of deviatoric strains. In this connection we comment that the measurements of plastic deformation-induced rotations and the determinations of crystal structure phases such as martensite *versus* austenite discussed by Robertson *et al.* (2007) for cyclic deformation of nitinol shape memory alloys are likely to be accurate. However, the magnitude of the deviatoric strains determined for cyclically deformed nitinol are likely to be significantly overestimated, especially in the highly distorted regions near crack tips.

**3.2.5. Microbeams in high-pressure science.** A new and important application for polychromatic and scanned monochromatic microbeam diffraction to high-pressure investigations of crystal structures (Wang *et al.*, 2010) has emerged recently. Nanoscale X-ray beams make it possible to avoid key limitations in the study of the structure of materials up to multi-megabar ( $>200\ \text{Mbar}$ , with  $1\ \text{bar} = 10^5\ \text{Pa}$ ) pressures, including spatially resolved measurements of multiple grains within a single sample, measurements of stress gradients, and searches for crystal domains on micrometre or submicrometre length scales within multi-micrometre grain sizes in diamond-anvil cells. Measurements on Fe, Pt and W were used as demonstrations with beam sizes of 250 and 600 nm and pressures of up to 282 GPa, showing that nanoscale X-ray beams enable single-grain X-ray diffraction studies at ultra-high pressures in polycrystalline samples of postperovskite, a high-pressure phase of  $\text{MgSiO}_3$ . A further important aspect of the use of microbeams in high-pressure studies is the ability to achieve higher pressures and more extreme conditions by allowing additional miniaturization of pressure cells.

The importance of submicrometre polychromatic and scanned monochromatic X-ray microdiffraction in high-pressure science was demonstrated through the discovery by Mao *et al.* (2010) that a small rhombohedral distortion from simple cubic existed in the high-pressure Ca III phase of Ca at 300 K and that a monoclinic distortion from simple cubic exists at 30 K. Powder pattern measurements showed the structure to be simple cubic, while exhaustive theoretical work showed clearly that lower-enthalpy orthorhombic and tetragonal phases should form the stable structure. Single-nanocrystal diffraction patterns resolved the (pseudo) simple cubic patterns into multiple twin spots associated with rhombohedrally (at 300 K) and monoclinically (at 30 K) distorted simple cubic phases. This result in turn resolved the unlikely implication that a simple cubic structure could form the stable high-pressure structure at low temperature.

## 4. Polychromatic 2DXM

### 4.1. Metal–insulator transition in VO<sub>2</sub>

Because it affords direct access to full crystal diffraction patterns without sample orientation issues, polychromatic microbeam Laue diffraction is becoming increasingly important for *in situ* investigations of the crystallographic structure, strain and structural phase transformations in systems such as metal–insulator transition materials, nanomechanically active materials, and both substrate-supported and self-supporting nanorods and nanoribbons. Tselev *et al.* (2011) combined submicrometre-resolution *in situ* 2DXM at the APS with optical imaging, resistivity measurements and numerical modeling. They showed that large reversible mechanical displacements observed in VO<sub>2</sub> nanoplatelets near the metallic–insulating phase-transition temperature are driven by a combination of large (~1%) lattice parameter differences between the monoclinic (insulating M2) and tetragonal (metallic rutile R) phases and a triangular domain pattern (see Fig. 10) that is induced by inhomogeneous Joule heating in narrow self-supporting nanoplatelet strips. As shown in Fig. 10,

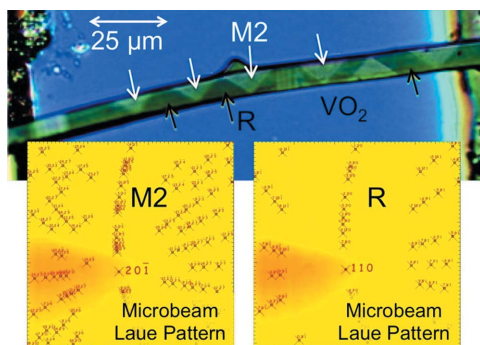


**Figure 10**

Optical image of a VO<sub>2</sub> nanoplatelet with lighter insulating monoclinic (M2 phase) and darker metallic tetragonal (R phase) domains. The domains are self-organized during current passage into triangular shapes by Joule heating. The Laue diffraction patterns at the bottom of the figure taken with a 0.5 μm-diameter polychromatic microbeam demonstrated that the two types of domains coexist within the VO<sub>2</sub> nanoplatelet. Adapted from Tselev *et al.* (2011) with permission.

X-ray microdiffraction provided lattice structure and strain measurements inside individual 5–10 μm phase domains. Such information is important for understanding the underlying physics of interactions between lattice structure and electronic properties in metal–insulator materials and important for possible development of room-temperature nanoactuator applications.

In related VO<sub>2</sub> work, Cao *et al.* (2010) used *in situ* submicrometre-resolution 2DXM at the ALS to map the temperature–strain–phase space of VO<sub>2</sub> and identified the presence of M2-phase Laue diffraction spot splitting as the result of twinning during tensile straining of VO<sub>2</sub> on a substrate. Their work emphasized the ability to exploit lattice strain in micro- and nanoscale electronic materials to access fundamental physics that is not available in bulk forms of materials such as VO<sub>2</sub>. The above investigations suggest a vital role for polychromatic X-ray microscopy with submicrometre spatial resolution for the identification of crystal phases and phase changes in correlated electron materials, and even more so as sub-100 nm resolution becomes available.

### 4.2. Evolution of strain in Al interconnect lines during electromigration

Electromigration is an atomic diffusion process driven by high electrical current densities in electronic device interconnect wires. In microelectronics, electromigration can cause failure when a divergence in the mass flux creates voids or extrusions resulting in open or short circuits. As component dimensions decrease, current densities increase, making electromigration increasingly important as a failure mechanism. Several studies have used 2DXM in both polychromatic and scanned monochromatic modes at the ALS and APS to explore this process in Al and Cu interconnect lines (Zhang *et al.*, 2008; Zhang & Cargill, 2011; Chen *et al.*, 2008; Budiman *et al.*, 2006). Zhang *et al.* (2008) measured the deviatoric and full elastic strains in passivated Al lines with near-bamboo structures at a temperature of 463 K, both before and during application of a current density of about  $1.5 \times 10^6$  A cm<sup>-2</sup>. The measurements showed the development of a strong strain gradient in the upstream part of the Al lines but no strain gradient in the downstream part. By comparison with the strain measurements, model calculations carried out using both an Eshelby model and finite element methods showed that electromigration occurs primarily along the top and bottom interfaces of the passivated wire, with less flux near the edges of the line than near the center. Evidence of plastic deformation was observed in the diffraction patterns, and the magnitude of the strain gradient allowed the effective valence of the diffusing species to be determined. Higher-spatial-resolution 2DXM (below 100 nm) will be required in order to study the complex deformation microstructure (Spolenak *et al.*, 2003) in circuits that more closely approximate those found in real systems.

### 4.3. Whisker growth in Pb-free Sn films

Although pure tin is now widely used as an environmentally important lead-free substitute for terminal plating in elec-

tronic devices, its propensity for forming metallic whiskers that can cause device failure makes the complex whisker formation process a critical technological issue. Sobiech *et al.* (2009) have used polychromatic 2DXM to investigate strain distributions around Sn whiskers generated following deposition and aging of pure tin on copper substrates. They concluded that local in-plane strain gradients observed around the root of Sn whiskers combine with previously reported out-of-plane strain depth gradients (Sobiech *et al.*, 2008) as driving forces for whisker growth.

On the other hand, recent investigations by Pei *et al.* (2012) suggest that the growth of whiskers in electronic devices is a much richer, multifaceted, materials evolution issue requiring more comprehensive *in situ* investigations, with detailed characterization required at all stages of evolution. Moreover, zinc, cadmium, indium and silver are also known to form whiskers under such conditions. The apparent complexity of the materials evolution on mesoscopic length scales suggests that 3DXM with sub-100 nm resolution and comprehensive grain size, orientation and full strain tensors (deviatoric and dilatational) in addition to complementary microscopy tools such as electron backscattering microscopy (Pei *et al.*, 2012) will be required to elucidate the underlying materials issues.

#### 4.4. Epitaxial oxide buffer layer film growth

2DXM was used by Budai *et al.* (2003) to study the detailed mechanisms of epitaxial growth and crystallographic orientations of a 0.5  $\mu\text{m}$ -thick  $\text{CeO}_2$  film on a roll-textured Ni substrate. Penetrating polychromatic X-ray beams probed the substrate as well as the film with  $\sim 0.01^\circ$  angular resolution, elucidating epitaxy on a grain-by-grain basis. Pole figures for fuzzy (diffuse) film Bragg reflections and sharp substrate Bragg peaks showed directly that the cubic  $\text{CeO}_2$  films grew epitaxially, but with up to a  $5.3^\circ$  out-of-plane rotation and a  $45^\circ$  in-plane rotation. The out-of-plane rotation systematically aligned the  $\text{CeO}_2$  orientation closer to the surface normal than the  $\sim \pm 5^\circ$  distribution of the Ni alignments with the surface normal. Similar studies of YBCO superconductors on a  $\text{CeO}_2$  buffer showed that such sharper film texturing leads to larger percolative superconducting regions because low-angle boundaries ( $< 5^\circ$ ) yield enhanced critical current densities (Specht *et al.*, 2007). Moreover, the tilt mechanisms observed in these studies are probably important in heteroepitaxial material systems in general, such as thermal barriers, solar cells or corrosion-resistant coatings.

### 5. Outlook for submicrometre-resolution polychromatic three-dimensional X-ray microscopy

The 3DXM technique discussed here is one of a number of new and innovative high-spatial-resolution X-ray probes that have been developed to exploit the high brilliance of X-ray beams at synchrotron facilities around the world. These advanced probes for investigating the crystal structure, underlying microstructure and evolution of materials are available to users at all levels through a competitive proposal process. In general, however, these techniques are at or near

the cutting edge of development and are often conducted in connection with experienced collaborators in addition to beamline scientists. As the instruments and the underlying control and analysis software mature, entirely new levels of scientific investigation can be expected from all of these techniques.

Strong scientific drivers exist for the development of polychromatic and scanned monochromatic 3DXM in the sub-100 nm-resolution range. Resolution improvements in this range are in progress, which will make it possible to address specific materials issues such as local strains associated with dislocation pileups at grain boundaries and defect microstructure more directly and definitively. Further examples would include dislocation cell wall physics in ductile deformation, local stresses and tractions associated with grain boundaries in polycrystalline materials, local stresses/strains associated with the deleterious growth of metallic whiskers in Sn solders, deformation fields and the underlying science associated with nano- and micro-indentation of metals and semiconductors, and the complex and collective interactions associated with dislocation multiplication, dislocation density fluctuations and the subsequent aggregation into microstructural features.

Continued advancements can be expected in X-ray focusing optics, depth-profiling techniques, the speed and energy resolution of large-scale X-ray area detectors, the computational and data-handling infrastructure, 3DXM data analysis, and three-dimensional display and visualization software. Such developments will provide capabilities for new levels of direct and quantitative comparisons between nanoscale 3DXM measurements and model simulations such as finite element simulation of deformation and microstructure evolution and the increasingly powerful first-principles simulation approaches. It is perhaps here, at the confluence of theory-driven simulations and spatially resolved experimental measurements, where the greatest impact on both our fundamental understanding of the underlying science of materials and the generation of new technological materials applications will be realized over the coming decades.

The expected advances in spatial resolution, detector technology and data analysis techniques associated with 3DXM, including automated data analysis, will provide the basis for increasingly sophisticated mesoscale investigations bridging nanoscale to macroscale materials science. Moreover, such advances can be expected to have even larger impacts on both materials science and related scientific disciplines as 3DXM techniques mature into a suite of tools that can be used routinely by scientists and engineers without specialized diffraction and analysis expertise.

This review was supported at Oak Ridge National Laboratory (BCL) by the US Department of Energy (DOE), Office of Basic Energy Sciences, as part of the Center for Defect Physics in Structural Materials Energy Frontier Research Center and at the National Institute for Standards and Technology (LEL) by the US Department of Commerce.

References

- Argon, A. S. & Haasen, P. (1993). *Acta Metall. Mater.* **41**, 3289–3306.
- Barabash, R. I., Bei, H., Gaob, Y. F. & Ice, G. E. (2011). *Scr. Mater.* **64**, 900–903.
- Barabash, R., Ice, G. E., Larson, B. C., Pharr, G. M., Chung, K.-S. & Yang, W. (2001). *Appl. Phys. Lett.* **79**, 749–751.
- Bei, H., Shim, S., Pharr, G. M. & George, E. P. (2008). *Acta Mater.* **56**, 4762–4770.
- Budai, J. D., Liu, W., Tischler, J. Z., Pan, Z. W., Norton, D. P., Larson, B. C., Yang, W. & Ice, G. E. (2008). *Thin Solid Films*, **516**, 8013–8021.
- Budai, J. D., Yang, E., Tamura, N., Chung, J.-S., Tischler, J. Z., Larson, B. C., Ice, G. E., Park, C. & Norton, D. P. (2003). *Nat. Mater.* **2**, 487–492.
- Budiman, A. S., Han, S. M., Greer, J. R., Tamura, N., Patel, J. R. & Nix, W. D. (2008). *Acta Mater.* **56**, 602–608.
- Budiman, A. S., Tamura, N., Valek, B. C., Gadre, K., Maiz, J., Spolenak, R., Nix, W. D. & Patel, J. R. (2006). *Appl. Phys. Lett.* **88**, 233515.
- Cao, J., Gu, Y., Fan, W., Chen, L. Q., Ogletree, D. F., Chen, K., Tamura, N., Kunz, M., Barrett, C., Seidel, J. & Wu, J. (2010). *Nano Lett.* **10**, 2667–2673.
- Chao, J., Mark, A., Fuller, M. L. S., McIntyre, N. S., Holt, R. A., Klassen, R. J. & Liu, W. (2009). *Mater. Sci. Eng. A*, **524**, 20–27.
- Chen, K., Kunz, M., Tamura, N. & Wenk, H.-R. (2011). *Eur. J. Mineral.* **23**, 169–178.
- Chen, K., Tamura, N., Valek, B. C. & Tu, K. N. (2008). *J. Appl. Phys.* **104**, 013513.
- Chung, J.-S. & Ice, G. E. (1999). *J. Appl. Phys.* **86**, 5249–5255.
- Durst, K., Backes, B. & Göken, M. (2005). *Scr. Mater.* **52**, 1093–1097.
- El-Azab, A. (2000). *Phys. Rev. B*, **61**, 11956–11966.
- Feng, G., Budiman, A. S., Nix, W. D., Tamura, N., Patel, J. R. (2008). *J. Appl. Phys.* **104**, 043501.
- Greer, J. R. & Nix, W. D. (2006). *Phys. Rev. B*, **73**, 245410.
- Hahner, P. & Zaiser, M. (1999). *Mater. Sci. Eng. A*, **272**, 443–454.
- Hu, X., Wei, C., Margolin, H. & Nourbakhsh, S. (1992). *Scr. Metal. Mater.* **27**, 865–870.
- Ice, G. E., Budai, J. D. & Pang, J. W. L. (2011). *Science*, **334**, 1234–1239.
- Kassner, M. E., Geantil, P. & Levine, L. E. (2012). *Int. J. Plast.* In the press. doi:10.1016/j.ijplas.2012.10.003.
- Kelkar, A., Roth, R. & Clark, J. (2001). *JOM*, **53**, 28–32.
- Kröner, E. (1981). *Physics of Defects*, edited by R. Balian, M. Kleman & J. Poirier, pp. 282–315. Amsterdam: North-Holland.
- Kubin, L. (1993). *Materials Science and Technology*, Vol. 6, pp. 137–190. Weinheim: VCH.
- Larson, B. C., El-Azab, A., Yang, W., Tischler, J. Z., Liu, W. & Ice, G. E. (2007). *Philos. Mag.* **87**, 1327–1347.
- Larson, B. C., Tischler, J. Z., El-Azab, A. & Liu, W. (2008). *J. Eng. Mater. Technol.* **130**, 021024.
- Larson, B. C., Yang, W., Ice, G. E., Budai, J. D. & Tischler, J. Z. (2002). *Nature (London)*, **415**, 887–890.
- Levine, L. E., Geantil, P., Larson, B. C., Tischler, J. Z., Kassner, M. E. & Liu, W. (2012). *J. Appl. Cryst.* **45**, 157–165.
- Levine, L. E., Geantil, P., Larson, B. C., Tischler, J. Z., Kassner, M. E., Liu, W., Stoudt, M. R. & Tavazza, F. (2011). *Acta Mater.* **59**, 5803–5811.
- Levine, L. E., Larson, B. C., Yang, W., Kassner, M. E., Tischler, J. Z., Delos-Reyes, M. A., Fields, R. J. & Liu, W. (2006). *Nat. Mater.* **5**, 619–622.
- Liu, C., Ice, G. E., Liu, W., Assoufid, L., Qian, J., Shi, B., Khachatryan, R., Wiecezorek, M., Zschack, P. & Tischler, J. Z. (2012). *Appl. Surf. Sci.* **258**, 2182–2186.
- Maaß, R., Van Petegem, S., Ma, D., Zimmermann, J., Grolimund, D., Roters, F., Van Swygenhoven, H. & Raabe, D. (2009). *Acta Mater.* **57**, 5996–6005.
- Magid, K. R., Florando, J. N., Lassila, D. H., LeBlanc, M. M., Tamura, N. & Morris, J. W. Jr (2009). *Philos. Mag.* **89**, 77–107.
- Mao, W. L., Wang, L., Ding, L., Yang, W., Liu, W., Kim, D. Y., Luo, W., Ahuja, R., Meng, Y., Sinogeikin, S., Shu, J. & Mao, H.-K. (2010). *Proc. Natl Acad. Sci. USA*, **107**, 9965–9968.
- Mughrabi, H. (1983). *Acta Metall.* **31**, 1367–1379.
- Mughrabi, H. & Ungár, T. (2002). *Dislocations in Solids*, edited by F. R. N. Nabarro & M. S. Duesbery, Vol. 11, pp. 345–411. Amsterdam: North-Holland.
- Mughrabi, H., Ungár, T., Kienle, W. & Wilkens, M. (1986). *Philos. Mag. A*, **53**, 793–813.
- Needlemann, A. & Sevillano, J. G. (2003). *Scr. Mater.* pp. 109–111.
- Nye, J. F. (1953). *Acta Metall.* **1**, 153–162.
- Olmsted, D. L., Holm, E. A. & Foiles, S. M. (2009). *Acta Mater.* **57**, 3704–3713.
- Pang, J. W. L., Ice, G. E. & Liu, W. (2010). *Mater. Sci. Eng. A*, **528**, 28–31.
- Pei, F., Jadhav, N. & Chason, E. (2012). *Appl. Phys. Lett.* **100**, 221902.
- Polvino, S. M., Valek, B. C., Tamura, N. & Robach, O. (2012). *XMAS Tutorial v.1*, <http://xraysweb.lbl.gov/microdif/downloads/XMAS%20Manual%20v1.pdf>.
- Poshadel, A., Dawson, P. & Johnson, G. (2012). *J. Synchrotron Rad.* **19**, 237–244.
- Poulsen, H. F. (2004). *Three-Dimensional X-ray Diffraction Microscopy: Mapping Polycrystals and Their Dynamics*. Berlin: Springer-Verlag.
- Poulsen, H. F., Jensen, D. J. & Vaughan, G. B. M. (2004). *MRS Bull.* **29**, 166–169.
- Robertson, S. W., Mehta, A., Pelton, A. R. & Ritchie, R. O. (2007). *Acta Mater.* **55**, 6198–6207.
- Rollett, A. D., Brahme, A. P. & Roberts, C. G. (2007). *Mater. Sci. Forum*, **558–559**, 33–42.
- Sobiech, M., Welzel, U., Mittemeijer, E. J., Hügel, W. & Seekamp, A. (2008). *Appl. Phys. Lett.* **93**, 011906.
- Sobiech, M., Wohlschlögel, M., Welzel, U., Mittemeijer, E. J., Hügel, W., Seekamp, A., Liu, W. & Ice, G. E. (2009). *Appl. Phys. Lett.* **94**, 221901.
- Specht, E. D., Goyal, A. & Liu, W. (2007). *J. Mater. Res.* **22**, 664–674.
- Spolenak, R., Brown, W. L., Tamura, N., MacDowell, A. A., Celestre, R. S., Padmore, H. A., Valek, B., Bravman, J. C., Marieb, T., Fujimoto, H., Batterman, B. W. & Patel, J. R. (2003). *Phys. Rev. Lett.* **90**, 096102.
- Spolenak, R., Ludwig, W., Buffiere, J. Y. & Michler, J. (2010). *MRS Bull.* **35**, 368–374.
- Thomson, R. & Levine, L. E. (1998). *Phys. Rev. Lett.* **81**, 3884–3887.
- Tsejov, A., Budai, J. D., Strelcov, E., Tischler, J. Z., Kolmakov, A. & Kalinin, S. V. (2011). *Nano Lett.* **11**, 3065–3073.
- Uchic, M. D., Dimiduk, D. M., Florando, J. N. & Nix, W. D. (2004). *Science*, **305**, 986–989.
- Ungár, T., Mughrabi, H., Rönnpögel, D. & Wilkens, M. (1984). *Acta Metall.* **32**, 333–342.
- Wang, L., Barabash, R. I., Yang, Y., Bieler, T. R., Crimp, M. A., Eisenlohr, P., Liu, W. & Ice, G. E. (2011). *Metall. Mater. Trans. A*, **42**, 626–635.
- Wang, L., Ding, Y., Yang, W., Liu, W., Cai, Z., Kung, J., Shu, J., Hemley, R. J., Mao, W. L. & Mao, H.-K. (2010). *Proc. Natl Acad. Sci. USA*, **107**, 6140–6145.
- Yang, W., Larson, B. C., Ice, G., Tischler, J., Budai, J., Chung, K. S. & Lowe, W. (2003). *Appl. Phys. Lett.* **82**, 3856–3858.
- Yang, W., Larson, B. C., Pharr, G. M., Ice, G. E., Budai, J. D., Tischler, J. Z. & Liu, W. (2004). *J. Mater. Res.* **19**, 66–72.
- Yang, W., Larson, B. C., Tischler, J. Z., Ice, G. E., Budai, J. D. & Liu, W. (2004). *Micron*, **35**, 431–439.
- Zaiser, M. & Moretti, P. (2005). *J. Stat. Mech. Theory Exp.* **8**, P08004.
- Zaiser, M. & Seeger, A. (2002). *Dislocations in Solids*, edited by F. R. N. Nabarro & M. S. Duesbery, Vol. 11, pp. 2–100. Amsterdam: North-Holland.
- Zhang, H. & Cargill, G. S. III (2011). *J. Mater. Res.* **26**, 498–502.
- Zhang, H., Cargill, G. S. III, Ge, Y., Maniatty, A. M. & Liu, W. (2008). *J. Appl. Phys.* **104**, 123533.